Journal of Applied Geodesy 3 (2009), 231–238 © de Gruyter 2009. DOI 10.1515/JAG.2009.023

Deformation analysis of the unified lunar control networks

H. Bâki Iz, Yong Qi Chen, Bruce Anthony King, Xiaoli Ding and Chen Wu

Abstract. This study compares the latest Unified Lunar Control Network, ULCN 2005, solution with the earlier ULCN 1994 solution at global and local scales. At the global scale, the relative rotation, translation, and deformation (normal strains and shears) parameters between the two networks are estimated as a whole using their colocated station Cartesian coordinate differences. At the local scale, the network station coordinate differences are examined in local topocentric coordinate systems whose origins are located at the geometric center of quadrangles and tetrahedrons. This study identified that the omission of the topography in the old ULCN solutions shifted the geometric center of the lunar figure up to 5 km in the lunar equatorial plane and induced a few hundred-meter level global rotations of the ULCN 1994 reference frame with respect to ULCN 2005. The displacements between the old and new control networks are less than ± 2 km on the average at the local scale, which behave like translations, caused by the omission of lunar topography in the earlier solution. The contribution of local rigid body rotations and dilatational and compressional components to the local displacements are approximately ± 100 m for a quadrangle/tetrahedron of an average side length of 10 km.

Keywords. Lunar control network, ULCN 2005, lunar topography, network deformations.

1. Introduction

As in the case of the Earth, Lunar mapping activities require a reference network for the selenodetic control. The recent lunar control networks include the Unified Lunar Control Network (ULCN 1994) and the Clementine Lunar Control Network (CLCN), both derived at RAND (Davies et al. 1987), and ULCN 2005 at USGS (Archinal et al. 2006). The ULCN 1994 was based on images from the Apollo, Mariner 10, and Galileo missions, and Earth-based photographs, whereas the CLCN was derived from Clementine images and measurements on Clementine 750-nm images (Edwards et al. 1996). Further information about these solutions can be found in the USGS Astrogeology site (USGS Control Networks 2008).

ULCN 2005 is the fusion of the ULCN 1994 and CLCN improving significantly upon the accuracy of the CLCN. The primary feature of the ULCN 2005 in comparison to the previous networks is due to the inclusion of the radii of the control points in the solution. Hence, the resulting ULCN 2005 is a unified three dimensional photogrammetrically determined network, which consists of 272,931 control points with an average of one point for every approximately 46 km^2 (Archinal et al. 2006). Comparison by Archinal et al. 2006 revealed that the radii derived from the images show no systematic difference compared to those from the Clementine LIDAR values (Smith et al. 1997), which implies that the radii must be of a few hundred meters accuracy. The horizontal accuracy of the ULCN 2005 is also reported to be a few hundred meters (Archinal et al. 2006).

The most straightforward comparison of the old and new control networks is to examine the differences in the Cartesian and radial components of the colocated control points (ibid). Nonetheless, although the magnitude and the distribution of the differences are informative, they do not reveal the nature of the underlying systematic differences between the two networks. In this study, the network distortions described by the differences between the ULCN 2005 and the ULCN 1994 Cartesian coordinates are analyzed as a function of relative rigid body motions (rotations and translations) and deformations (normal strains and shears) at a global scale. At the local scale, the control point differences of 243,676 quadrangles (for the ULCN 1994) and tetrahedrons (for the ULCN 2005) formed by four colocated lunar control points are modeled in their respective topocentric coordinate systems and investigated to reveal the underlying properties of the local distortions.

2. The lunar reference system

Lunar control networks can be referenced to two slightly different lunar body-fixed coordinate systems: a mean Earth/rotation system, and a principal axis system (Roncoli 2005). The mean Earth/rotation system (also called the mean Earth/polar axis system) is based upon a mean direction to the Earth and a mean axis of rotation of the Moon. The principal axis system is also a lunar body-fixed coordinate system aligned with the principal axes of the Moon. The principal axes and the mean Earth/rotation axes of the Moon do not coincide but differ by less than 1 km because the Moon is not really a synchronously rotating triaxial ellipsoid (ibid). In this system, the mean Earth equator is defined at J2000 with the origin at the center of mass of the Moon. The selenocentric latitudes are measured from the center of the Moon relative to the equator and longitudes are measured from 0–360 degrees, positive to the east. Nearly all lunar maps depict longitudes as 0–180 degrees east and west as is done on terrestrial maps.

The fusion of CLCN and ULCN 1994 data and the use of Clementine a priori spacecraft position data in the mean Earth/polar axis system suggests that ULCN 2005 is referenced to the same mean Earth/polar axis system as reported in Davies et al. 1994, (Archinal et al. 2006). Nonetheless, as it will be shown in the following sections, that this is not the case for the old ULCN 1994 solution. Evidently, the omission of the topography in the ULCN 1994 solution had an impact on the origin and orientation of its reference frame as realized by the network station coordinates.

3. Methodology: deformations of a polyhedron

In order to investigate the network distortions, i.e. the differences between the Cartesian coordinates of the new ULCN 2005 solution with the earlier ULCN 1994 solution, the classical tools of deformation analyses are deployed. First, the relative rotation, translation and deformation (normal strains and shears) parameters between the two networks whose control points are the vertices of a polyhedron are considered. At the local scale, the network differences of quadrangles/tetrahedrons are modeled and investigated to reveal the underlying properties of the control points coordinate differences as local deformations in their topocentric coordinate systems.

The following formulations are used for both global and local analysis. The underlying mathematical foundations of the analysis, namely the theory of deformations, are exhaustively discussed by Novozhilov (1961). An operational summary of its use in geodesy is given by Grafarend (1982). Studies by Schön (2007) and Cai et al. (2008) are some of the most recent examples of its applications in deformation analysis of geodetic control networks in time domain.

Consider the Cartesian displacement components, u, v, w of a point subject to deformation, which are defined in terms of its Cartesian position X, Y, Z before the deformation, and x, y, z after the deformation as

$$\begin{aligned} u &:= X - x, \\ v &:= Y - y, \\ w &:= Z - z. \end{aligned} \tag{1}$$

The displacement components expanded into Taylor series (neglecting second and higher order terms) are given by

$$\begin{aligned} u &= u_0 + u_x x + u_y y + u_z z, \\ v &= v_0 + v_x x + v_y y + v_z z, \\ w &= w_0 + w_x x + w_y y + w_z z. \end{aligned} \tag{2}$$

By definition

$$\begin{aligned} e_{xx} := u_x := \frac{\partial u}{\partial x}, \quad u_y := \frac{\partial u}{\partial y}, \quad u_z := \frac{\partial u}{\partial z} \\ v_x := \frac{\partial v}{\partial x}, \quad e_{yy} := v_y := \frac{\partial v}{\partial y}, \quad v_z := \frac{\partial v}{\partial z} \\ w_x := \frac{\partial w}{\partial x}, \quad w_y := \frac{\partial w}{\partial y}, \quad e_{zz} := w_z := \frac{\partial w}{\partial z} \end{aligned} \tag{3}$$

from which complete set of strain tensor elements are obtained as

$$\begin{aligned} e_{xy} = \frac{1}{2}(u_y + v_x), \quad e_{xz} = \frac{1}{2}(u_z + w_x), \\ e_{yz} = \frac{1}{2}(v_z + w_y), \\ \omega_{xy} = \frac{1}{2}(u_y - v_x), \quad \omega_{xz} = \frac{1}{2}(u_z - w_x), \\ \omega_{yz} = \frac{1}{2}(v_z - w_y). \end{aligned} \tag{4}$$

These expressions can be combined as follows:

$$\begin{aligned} u &= u_0 + u_x x + \frac{1}{2}(u_y + v_x)y + \frac{1}{2}(u_y - v_x)y \\ &\quad + \frac{1}{2}(u_z + w_x)z + \frac{1}{2}(u_z - w_x)z, \\ v &= v_0 + \frac{1}{2}(v_x + u_y)x + \frac{1}{2}(v_x - u_y)x + v_y z \\ &\quad + \frac{1}{2}(v_z + w_y)z + \frac{1}{2}(v_z - w_y)z, \\ w &= w_0 + \frac{1}{2}(w_x + u_z)x + \frac{1}{2}(w_x - u_z)x \\ &\quad + \frac{1}{2}(w_y + v_z)y + \frac{1}{2}(w_y - v_z)y + w_z z, \end{aligned} \tag{5}$$

or equivalently

$$\mathbf{u} = \mathbf{A} \cdot \mathbf{p} \tag{6}$$

where

$$\begin{aligned} \mathbf{A} &:= \begin{bmatrix} 1 & 0 & 0 & y & z & 0 & x & 0 & 0 & y & z & 0 \\ 0 & 1 & 0 & -x & 0 & z & 0 & y & 0 & x & 0 & z \\ 0 & 0 & 1 & 0 & -x & -y & 0 & 0 & z & 0 & x & y \end{bmatrix}, \\ \mathbf{p}^{\mathbf{T}} &:= [u_0 \;\; v_0 \;\; w_0 \;\; \omega_{xz} \;\; \omega_{yz} \;\; \omega_{zy} \;\; e_{xx} \;\; e_{yy} \;\; e_{zz} \;\; e_{xy} \;\; e_{xz} \;\; e_{yz}]^T, \\ \mathbf{u}^{\mathbf{T}} &:= [u \;\; v \;\; w]^T. \end{aligned} \tag{7}$$

In equation (7), u_0, v_0, w_0 are the shift parameters of between the undeformed and deformed state of a polyhedron, ω_x, ω_y, ω_z are the rotations, and e_{xx}, e_{yy}, e_{zz} and e_{xy}, e_{xz}, e_{yz} are the linear strain parameters (compression or dilatation and shear respectively) for small deformations with respect to unity. All the parameters can be calculated uniquely if the displacements of four points (vertices of a tetrahedron) are known. In this analysis, the coordinates of each point that appear in the coefficient matrix in equation (7) are referenced to the geometric center of a tetrahedron and are evaluated at nominal coordinate values of a Taylor expansion.

The above relationships, when expressed in terms of the linear strain parameters of the deformations (hence their geometric interpretations), are valid only for small deformations with reference to unity for the deformation parameters, not with reference to the small magnitude of the displacements. Otherwise, the geometric meaning of the strains is only a crude approximation in describing the deformations.

4. Global network distortions

The 12 global distortion parameters between the two networks are estimated using equation (7) as a mathematical model with 272,931 colocated network station Cartesian coordinate differences in a least squares sense. Table 1 lists the estimated translation parameters in meters. The rotation angles are similarly expressed as distances in meters along the lunar equator. The deformation parameters refer to changes in meters against a lunar sphere of radius 1737 km. The values within the parentheses are the standard deviations of the estimates calculated using a diagonal variance-covariance matrix where the standard deviations of the Cartesian coordinate components are assumed to be 200 m. The a posteriori variance of unit weight is not applied in calculating the standard deviations of the estimates because the lunar topography, which is non-stochastic, is intrinsically projected onto all the coordinate components. All the estimated parameters, except the translation in the z direction, are statistically significant at 5 and 1 percent significance levels. The ULCN 1994 data is already included in the ULCN 2005 solution, and the ULCN 2005 solution is not constrained to the lunar laser ranging stations (Archinal, private communications, 2008). Hence, the translation components in the x and y directions (corresponding to an origin shift in the xy plane) are caused largely by the omission of the topography in the old ULCN 1994 solution. Moreover, because the lunar figure deviates from a sphere (Table 2), the omission of the spheroidal excesses contributed to translations as well as deformations in the old ULCN 1994 solution, though the latter ones are less pronounced in magnitude. For instance, the signs and the magnitudes of the spheroidal axes a, b and c of the best fitting triaxial lunar figure parameters for ULCN 2005 solution (Table 2) suggest that the dilatations in the x and y directions and compression in the z direction are due to the 1736.7 km lunar spherical radius used in the ULCN 1994 solution. These results are in agreement with the estimated dilatation and compression parameters given in Table 1.

On one hand, the standard deviation of all the estimated parameters, except the translation components are extremely small (close to 1 meter when rounded). This is partly due to the large amount of data, but mostly because the new and old data sets are the same in both solutions but differ only by the solution methodology of ULCN 2005 that also account for the radial component. On the other hand, the standard deviations of the translation parameters are relatively large because the radial distances indicate a lunar figure that deviates from a sphere and contain topographic irregularities.

Table 1: Translation components are in meters. The rotation angles are expressed as distances in meters on the lunar equator and the deformations parameters refer to the changes in the spherical radius of the lunar figure in meters. The values in parentheses are the standard deviations of the estimates calculated using an a priori standard deviation of 200 m for the Cartesian coordinate components.

Translation u_0, v_0, w_0	Rotation $\omega_x, \omega_y, \omega_z$	Scale e_{xx}, e_{yy}, e_{zz}	Shear e_{xy}, e_{xz}, e_{yz}
−5232 (666)	241 (1)	1809 (1)	968 (1)
−2199 (666)	187 (1)	1129 (1)	−1720 (1)
31 (666)	698 (1)	−1463 (1)	−36 (1)

5. Local network distortions

At the local scale, the control networks are scrutinized in topocentric coordinate systems defined on the lunar sphere (Appendix) at the geometric center of each of the four ULCN 1994 and ULCN 2005 control points. Since the ULCN 1994 is defined only by the latitudes and longitudes of the control points and a fixed radial component (i.e. on the lunar sphere), the four control points are locally defined quadrangles with a plane approximation, whereas the same control points in the ULCN 2005 solutions form tetrahedrons because of the presence of topography in the unconstrained radial coordinates.

Table 2: Geometrically best fitting lunar figure parameters based on ULCN2005 solution data (Iz 2009). The units are in meters. The values within parentheses are the standard errors of the estimated parameters. The first values of each lunar figure belong to the non-selenocentric best fitting lunar figure solutions. N/A: Not applicable.

Figure	a	b	c	x_c	y_c	z_c	RMS
Triaxial	1737899 (9)	1737570 (9)	1735742 (7)	−658 (6)	−681 (6)	133 (5)	1754
Ellipsoid	1737811 (10)	1737595 (10)	1735710 (8)	0	0	0	2018
Rotational	1737737 (5)	N/A	1735741 (7)	−653 (6)	−682 (6)	133 (5)	1756
Ellipsoid	1737705 (6)	N/A	1736710 (8)	0	0	0	2018
Sphere	1736965 (6)	N/A	N/A	−645 (6)	−696 (7)	142 (6)	1868
	1736934 (4)	N/A	N/A	0	0	0	2117

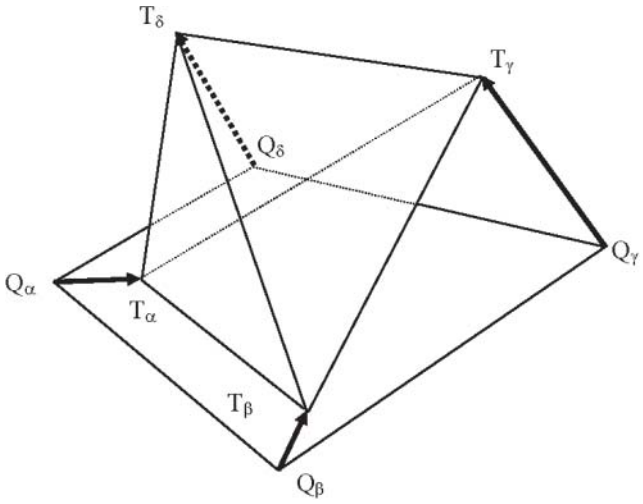

Figure 1: Distortion of quadrangles into tetrahedrons (or vice versa).

For the analysis, the quadrangles are established first by constructing over half a million Delaunay triangles using the 2D coordinates of a plate carrée projection of the ULCN 1994 control points, which are then combined with neighboring Delaunay triangles to form 271,530 quadrangles. The quadrangles' control points (vertices) in the ULCN 2005 form the corresponding 3D tetrahedrons (Figure 1). The curvilinear coordinates of the network control points are then converted into Cartesian coordinates. Subsequently, the local Cartesian coordinates of each quadrangle and tetrahedron vertices are calculated in their topocentric coordinate systems whose origins are defined by the average Cartesian components of each of the quadrangle's and tetrahedron's vertices using the relationships given in the appendix.

Although the exact solution for the rigid body motion and strain parameters are theoretically conceivable given the colocated Cartesian coordinates of the four control points in both ULCNs, there are numerical problems in inverting the coefficient matrix that appears in equation (7). The distribution of the control points is irregular, which causes near linear dependency between the rotation and shear parameter coefficients if some of the coordinate components are close to zero. For instance, if the x component of a control point is close to zero then the 4^{th} and the 10^{th} columns of the coefficient matrix are colinear, hence a numerically stable solution is not possible (there are additional scenarios that may lead to harmful colinearity). Separate solutions with and without the shear parameters showed that only less than 20% of the local deformations are subject to shear, whereas over 90 percent of quadrangles (243,676) are affected by rotations together with dilatation and compression, and rigid body translation parameters. Therefore, the following results are obtained in the absence of shears (i.e. using only 9 parameters) in a least squares sense with 3 degrees of freedom for each quadrangle and tetrahedron pair (a set of unique 3D Delaunay triangle solutions are also obtained using the same formulations with similar results). Note that it is possible to form more regular figures by selectively choosing control points for the analysis, but this approach will not only eliminate significant number of control points being examined but also the local distortional properties of the solutions will be smoothed out by using more control points distributed over larger areas.

The histograms and scatter plots in Figure 2 show that local rigid body motions, as translations are significant. Eighty percent of the changes in the radial component are concentrated within the interval ± 2 km and exhibit a normal distribution. This number is also in agreement with the RMS misclosures of about 1.7–2 km in the best fitting lunar figures computations (Table 2). The translations in northerly and easterly directions are also pronounced but not random. The magnitudes of the northerly components are at maximum on the limb of the lunar figure whereas the easterly translations are more pronounced on the far side of the moon.

In comparison, the contributions of all the rotation, dilatation and compression parameters that act like scale changes along the axes of the topocentric coordinate system, to the local displacements are markedly smaller (Figure 3 and Figure 4). They are within the ± 100 m range for a quadrangle/tetrahedron of an average side length of 10 km. Because the lunar topography does not vary significantly over areas of this size, the differences are more or less independent of the topography and therefore more representative of the effect of processing the data for the two network solutions.

6. Conclusion

This study identified and quantified that the omission of topography in the old ULCN solutions shifted the geometric center of the lunar figure up to 5 km in the lunar equatorial plane and induced a few hundred-meter level global rotations of the ULCN 1994 reference frame with respect to ULCN 2005 (Table 1).

Significant displacements between the old and new control networks are due to the omission of lunar topography in the earlier solution, which is, as expected, the dominant contributor in vertical displacements. Nonetheless, there are also significant horizontal translations of the control points of about ± 2 km (Figure 3). The contribution of rigid body rotations and local dilatational and compressional components to the local displacements are approximately ± 100 m for a quadrangle/tetrahedron of an average side length of 10 km (Figure 3 and 4), which are much less influenced by the omission of the topography in the ULCN 1994 solution. They are

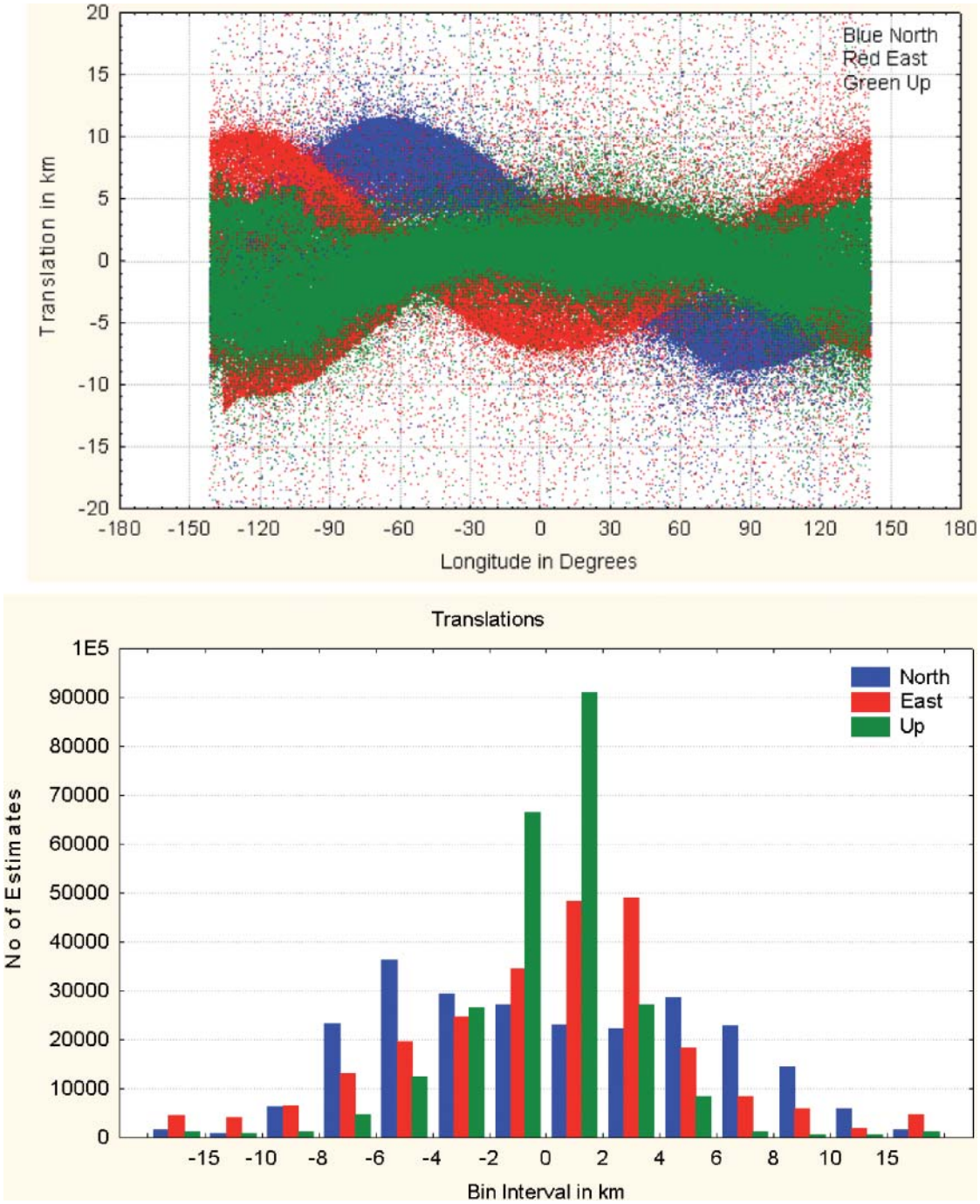

Figure 2: Distribution of the translation components as a function of the longitude of their topocentric coordinate systems' origins and their frequencies.

more representative of the processing differences between the control networks.

By the end of this year, satellite laser-altimetry measurements, which were recently carried out during the Chinese Chang'E 1 and the Japanese SELENE missions will be released to the scientific community. Moreover, recently launched lunar reconnaissance orbiter's (LRO) laser-altimeter (LOLA) will also provide abundant information about the lunar topography. The data from all the new missions are denser and more accurate than the ULCN 2005 data. The methods presented in this study also suit well analyzing their relative distortions.

7. Appendix: transformation from selenocentric to topocentric coordinate system

The selenocentric *Cartesian* coordinates of a station P (Figure 5) on or above the lunar sphere of radius

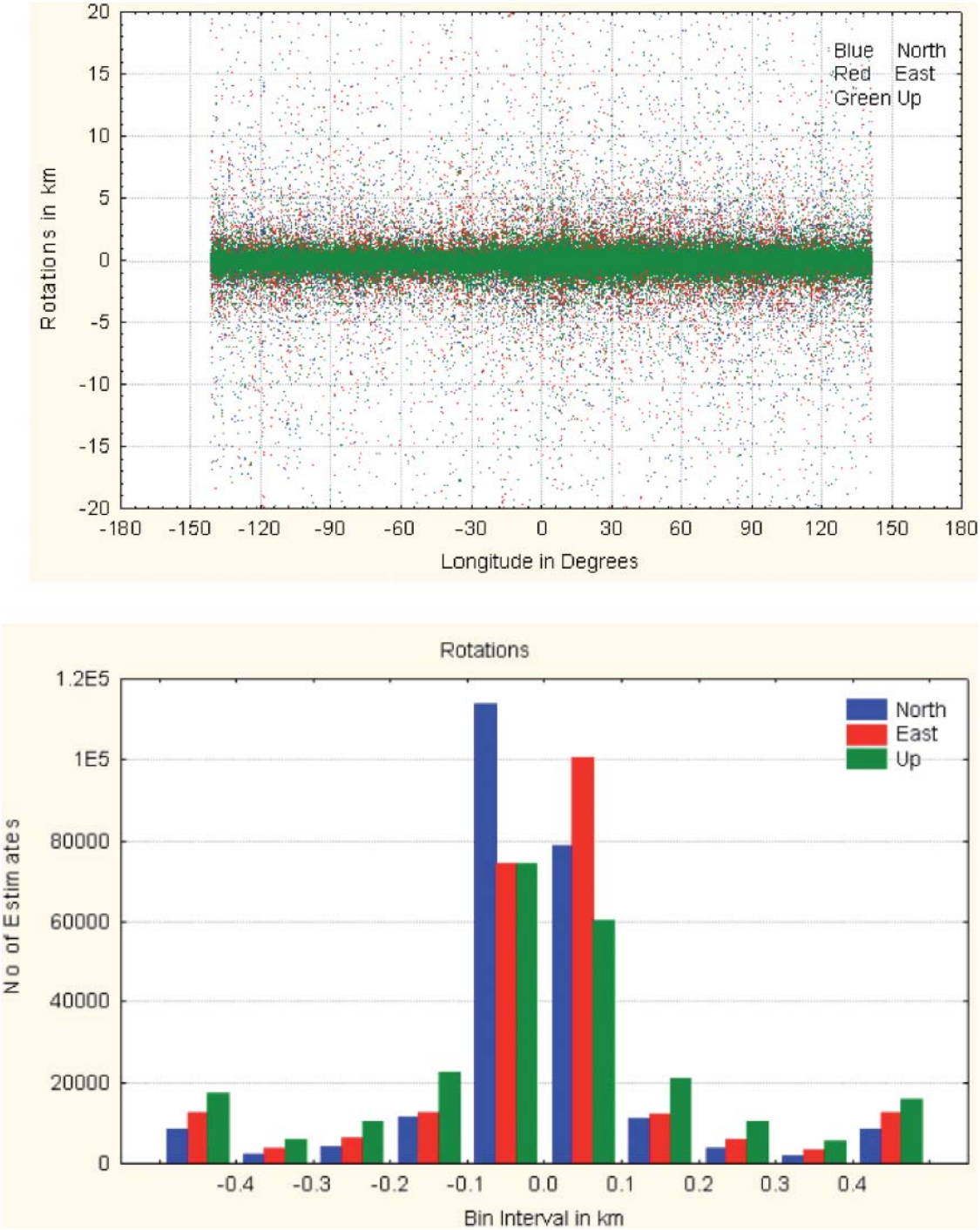

Figure 3: Distribution of the relative rotations between the quadrangles and the tetrahedrons about the North, East and Up axes as a function of the longitude of their topocentric coordinate systems' origins and their frequencies. The rotation angles are expressed in km for figures of an average side length 10 km.

R are given by

$$\begin{bmatrix} x_P \\ y_P \\ z_P \end{bmatrix} = \begin{bmatrix} (R+h_P)\cos\phi_P \cos\lambda_P \\ (R+h_P)\cos\phi_P \sin\lambda_P \\ (R+h_P)\sin\phi_P \end{bmatrix}. \quad (8)$$

The lunar topocentric coordinates of a point P in space $\mathbf{r_{T_P}} = (x_{T_P} \quad y_{T_P} \quad z_{T_P})^T$ can be calculated using the following transformation from the selenocentric to the lunar topocentric coordinate system:

$$\mathbf{r}_{T_P} = \mathbf{M}(\mathbf{r_P} - \mathbf{r_o}) \quad (9)$$

where ϕ_o, λ_o refers to the selenocentric latitude and longitude of the origin of the lunar topocentric coordinate system respectively (in this study, the origin is located at the geometric center of the quadrangle on the surface of the lunar sphere), and h_o and h_P are the heights of the station o and P on, above, or below the

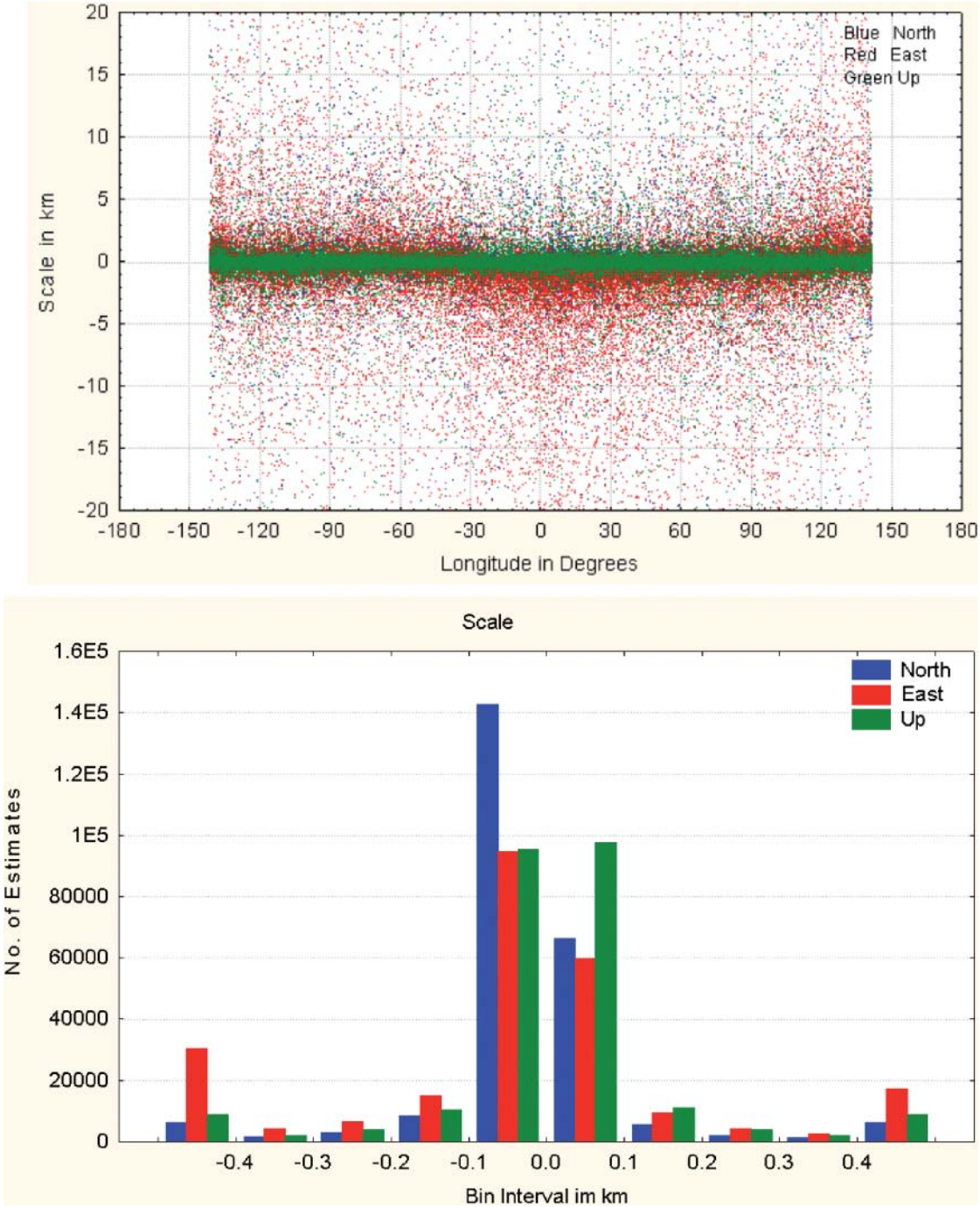

Figure 4: Distribution of three dilatation/compression components (scales also the North, East and Up axes) expressed in km over and average side length 10 km as a function of the longitude of their topocentric coordinate systems' origins and their frequencies.

lunar sphere. The position vectors of the origin of the lunar topocentric coordinate system and the point P are denoted by $\mathbf{r_o}$, $\mathbf{r_P}$. They are both in the selenocentric coordinate system and the rotation matrix $\mathbf{M}$ is given by

$$\mathbf{M} = \begin{bmatrix} -\sin\lambda_o & \cos\lambda_o & 0 \\ -\sin\phi_o\cos\lambda_o & -\sin\phi_o\sin\lambda_o & \cos\phi_o \\ \cos\phi_o\cos\lambda_o & \cos\phi_o\sin\lambda_o & \sin\phi_o \end{bmatrix}. \quad (10)$$

Acknowledgment

This study was supported by the Hong Kong Polytechnic University grants G-U417 and 1-BB83. UCLN 2005 data and pertinent details were provided by Brent Archinal from USGS, which is gratefully acknowledged. We wish to thank the two anonymous reviewers for their careful reading of the manuscript and their comments. Sections of this study were presented during the 6th European Congress on

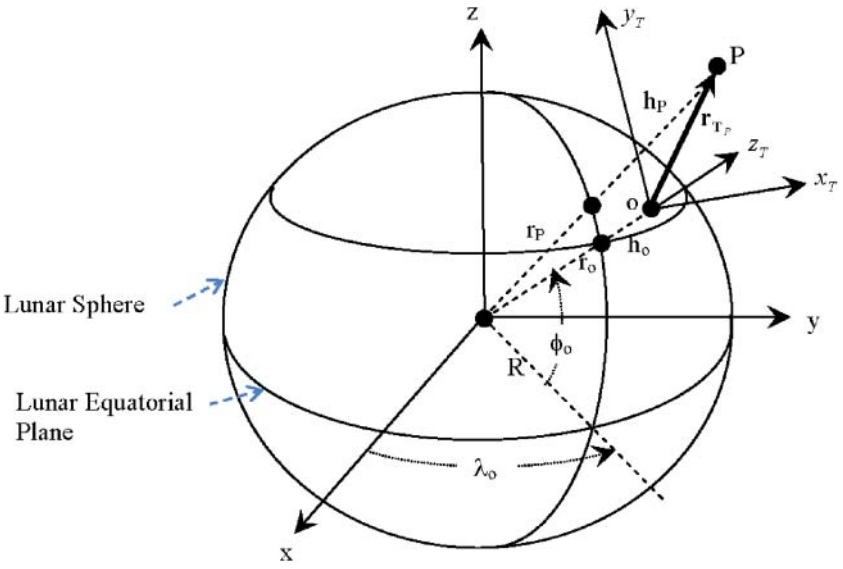

Figure 5: Selenocentric and lunar topocentric Cartesian coordinate systems.

Regional Geoscientific Cartography and Information Systems, in Munich, Germany, 2009.

References

Archinal, B. A., Rosiek, M. R., Kirk, R. L. and Redding, B. L., The Unified Lunar Control Network 2005, U.S. Geological Survey Open-File Report 2006-1367, http://pubs.usgs.gov/of/2006/1367/ (accessed Sep, 2006).

Cai, J., Wang, J., Wu, J., Hu, C., Grafarend, E. and Chen, J., Horizontal deformation rate analysis based on multi-epoch GPS measurements in Shanghai, Journal of Surveying Engineering, ACSE, 134:4(132), 2008.

Davies, M. E., Colvin, T. R., and Meyer, D. L., A unified lunar control network: the near side, JGR 92 (1987), 14177–14184.

Edwards, K. E., Colvin, T. R., Becker, T. L., Cook, D., Davies, M. E., Duxbury, T. C., Eliason, E. M., Lee, E. M., McEwen, A. S., Morgan, H., Robinson, M. S. and Sorensen, T., Global Digital Mapping of the Moon, Lunar Planet. Sci., XXVII: Houston, Lunar and Planetary Inst., 335, 1996.

Grafarend, E., Six Lectures on geodesy and global Geodynamics, Lecture II: Space Time Operational Geodesy, Pro. of the third int. Summer School in the Mountains, eds. H. Moritz and H. Sünkel, Mitt. Geod. Inst. TU Graz, Folge 41, Graz, 1982, 531–685.

İz, H. B., Geometrically Best Fitting Ellipsoids and Spheres of the Moon, Journal of Applied Geodesy 3 (2009), 155–162.

Novozhilov, V. V., Theory of Elasticity, New York: Pergamon Press, 1961.

Roncoli, R. B., Lunar Constants and Models Document JPL D-32296, 2005.

Schön, S., Affine Distortion of Small GPS Networks with Large Height Differences, GPS Solutions 11 (2007), 107–117.

Smith, D. E., Zuber, M. T., Neumann, G. A., and Lemoine, F. G., Topography of the Moon from the Clementine LIDAR, JGR 102: E1 (1997), 1591–1611.

USGS Control Networks, http://astrogeology.usgs.gov/Projects/ControlNetworks/ (accessed Nov, 2008).

Received: May 26, 2009 Accepted: Jun 16, 2009

Author information

H. Bâki Iz, Yong Qi Chen, Bruce Anthony King, Xiaoli Ding and Chen Wu
Department of Land Surveying and Geo-Informatics
The Hong Kong Polytechnic University
Hong Kong S.A.R., China
E-mail: lshbiz@polyu.edu.hk, lsyqchen@polyu.edu.hk, lsbaking@polyu.edu.hk, lsxlding@polyu.edu.hk, lswuchen@polyu.edu.hk